Journal of Hydraulic Structures
J. Hydraul. Struct., 2022; 8(4):1-16
DOI: 10.22055/jhs.2023.42219.1234

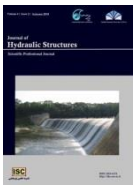

OPEN ACCESS

Optimization of the synthesis of UiO-66-NH_2 catalyst and its application for removing organophosphorus pesticides from wastewater

Abbas Mohammadi [1]
Mehdi Sedighi [2]
Mohsen Afsari [3]

Abstract

The present research focuses on optimizing the laboratory synthesis of a metal-organic framework for decomposing organophosphorus pollutants in aquatic environments (caused by pesticides). In the first stage, by defining and scoring five screening criteria, such as the price of raw materials, the complexity of the synthesis reaction, the efficiency of the catalyst, the possibility of industrial production (scalability), as well as the cost of the necessary equipment, the metal-organic framework 2-aminoterephthalate; oxygen (2-); zirconium (4+); tetrahydroxide was selected as the target catalyst. By considering the catalyst production yield as an objective function, the optimization of the most important variables affecting catalyst synthesis (reaction time, reaction temperature, amount of reaction solvent, type and amount of acid catalyst required, type and quantity of secondary solvent, and rotation speed of centrifuges) was discussed. The synthetic framework's structure has been confirmed by infrared spectroscopy and powder X-ray diffraction analyses. According to Brunauer-Emmett-Teller surface area analysis, the resulting catalyst has a specific area of 825 m^2/g and a mean pore diameter of 2.25 nm. This catalyst performed well in the laboratory in decomposing the selected organophosphorus pollutant (dimethyl nitrophenyl phosphate compound) with a half-life of 9 minutes.

Keywords: Organophosphate pesticide, Hydrolysis, Catalyst synthesis, Optimization, Metal-organic framework.

Received: 30 October 2022; Accepted: 16 January 2023

[1] Department of Chemical Engineering, University of Qom, Qom, Iran. Email: Mohammadi.a@qom.ac.ir **(Corresponding Author)**
[2] Department of Chemical Engineering, University of Qom, Qom, Iran.
[3] BIC Company, Qom, Iran.

1. Introduction

Insecticides are the most important group of pesticides. Worldwide, organophosphorus compounds account for about 40% of registered pesticides [1]. The insecticides are divided into three categories: high toxicity poisons (lethal dose (LD_{50}) =50 mg/kg, such as Parathion, used in agriculture), medium toxicity poisons (LD_{50}=50-1000 mg/kg, such as Coumaphos, used in animal husbandry), and low toxicity poisons (LD_{50}>1000 mg/kg, such as Malathion, which can be used in homes and gardens). It is clear from the variety of uses of these compounds that they have the potential to pollute water resources, soil resources [1-3], and livestock and agricultural products (such as grains and fruits [4, 5], meat and poultry [6], honey [7], etc.). Because these compounds are absorbed easily through various routes, such as the skin, mucous, digestive system, and respiratory system, poisoning caused by them is very common. Every year, thousands of people are treated for poisoning caused by these compounds [6, 8, 9]. Therefore, removing or neutralizing residual pollutants in water and soil environments or different products is extremely important.

Researchers have always considered removing these pollutants from water resources and environments a highly important task [10-16]. A phosphorus-oxygen double bond in the structure of organophosphorus pollutants and pesticides makes them highly susceptible to decomposition (hydrolysis). By attacking the phosphorus atom with a nucleophile agent (group), the phosphorus-oxygen double bond is weakened, and the pollutant molecule collapses structurally. The lack of phosphoester structure in decomposed compositions/compounds eliminates or reduces the destructive function of these poisons [17, 18].

The types of catalysts required for this hydrolysis process have been identified and produced through extensive research. It has become increasingly common to use metal-organic frameworks (MOFs) or porous coordination polymers in recent years because they offer desirable characteristics such as favorable temperature stability, favorable humidity stability, the ability to absorb and decompose a variety of chemical compounds, acceptable absorption and decomposition speeds, high absorption capacity, multi-use capability, high specific surface, great variety, as well as the ability to design and modify the molecular structure [19].

The MOF structures developed using metals from the fourth group of the periodic table (titanium Ti, zirconium Zr, and hafnium Hf) show excellent catalytic properties when decomposing and hydrolyzing phosphorus-oxygen, phosphorus-fluorine, and phosphorus-sulfur bonds [20]. While Bis {[1,3,5-benzènetricarboxylato (3-)-κ2O1, O3] cuprate(1-)} de cuivre(2+) copper benzene-1,3,5-tricarboxylate (HKUST-1 or Cu-BTC), NH_2-MIL-53(Al) and NH_2-MIL-101(Al) contain copper and aluminum metals in their structures, their Lewis acid properties allow them to decompose these pollutants catalytically. However, these structures are unstable against water (moisture), which limits their practical application [20, 21]. The MIL-101(Cr) metal-organic framework was modified with dialkylaminopyridine in 2013, resulting in the MIL-101/DAAP framework. This modification aimed to optimize pollutant decomposition half-life time. Under improved conditions, the modified metal-organic framework hydrolyzes diethyl 4-nitrophenyl phosphate with a half-life of 5 hours. As a result of the amine group within the ligand of this structure, the Brønsted base property is formed, and hydrolysis occurs [21, 22]. Due to their excellent stability against water (moisture) and air, zirconium-based synthesized frameworks are of great interest. In these structures, zirconium is highly susceptible to hydrolysis of organophosphorus due to the strong bond between zirconium and oxygen [21].

Various structures based on zirconium metal have been developed, the most important of which are PCN-222, NU-1000, and 2-aminoterephthalate; oxygen (2-); zirconium (4+); tetrahydroxide (UiO-66-NH_2) in the hydrolysis of organophosphorus. As a result of its

terephthalic acid ligand and zirconium nodes, UiO-66-NH_2 is capable of decomposing organophosphorus pollutants more rapidly than another zirconium base MOFs. The porphyrin ligands present in frameworks such as NU-1000 and PCN-222 make them susceptible to structural destruction due to their need to activate frameworks. However, the UiO-66-NH_2 can be easily activated due to its stable 2-aminoterephthalic acid ligand and strong bonding between its organic ligand and zirconium metal [23-25]. From an industrial point of view, UiO-66-NH_2 catalysts can also be synthesized on a commercial scale [26-28]. As shown in Table 1, PCN-222, NU-1000, and UiO-66-NH_2 have been compared based on efficiency, production, and economic factors. The UiO-66-NH_2 framework was further investigated in the present study to investigate the removal of organophosphorus pollutants.

Table 1. The screening of the most important metal-organic zirconium base frameworks for the degradation of organophosphorus pollutants

Catalyst structure	Price of the raw materials (18%)*	Access to raw materials (12%)	The complexity of the synthesis reaction (18%)	Cost of the necessary equipment (6%)	The efficiency of the catalyst (23%)	Possibility of the industrial production (23%)	Total score
UiO-66-NH_2	3**	4	3	4	4	3	3.41
NU-1000	1	1	2	3	4	3	2.45
PCN-222	4	2	2	1	2	2	2.30

* Index attractiveness percentage

** Relative score in the assessed index (1 is the lowest score, and 4 is the highest score)

The existing methods in the synthesis of MOF structures can be categorized into seven main categories: solvent evaporation method, diffusion method, electrochemical method, solvothermal method (thermal solvent), microwave synthesis method, physico-chemical method, and sonochemical method. Due to its favorable controllability, suitable reproducibility, and acceptable synthesis speed, solvothermal is the most suitable method for synthesizing the targeted catalyst [27, 28].

The diffusion method is not suitable for commercial production due to its low speed and high cost. The solvent evaporation method is also very time-consuming, and the uniformity of catalyst production depends on many variables, making reproducibility and control of the synthesis process difficult. It is difficult to control how crystals are formed, how large the crystals are, or other catalyst characteristics in the microwave method, even with the short reaction time. Physical mixing does not produce crystals with ideal structures. Solvothermal reactions produce a wide range of MOFs with different pore sizes by varying the reaction conditions, such as temperature, concentration, the ratio of organic ligands and metal salts, solubility of the reactants in the solvent, and pH of the synthesis mixture. Changing the synthesis variables can also create a specific catalyst with different porosities. Controlling the variables will also change the size of crystals, the way the links are connected, and the structure of the synthesized framework [26-29].

The review of the literature shows that the variables governing the solvothermal method influence the quality, quantity, and performance of the synthesized metal-organic structures, which have been not explored in previous studies. Therefore, unlike the previous studies, the main emphasis in this work is placed on the optimization of the most important variables

affecting the solvothermal method in synthesizing the UiO-66-NH_2 structure. A key objective of the current optimization study is to improve catalyst production efficiency in the synthesis process, accelerate commercialization, and reduce catalyst production costs. In addition, the half-life time of an organophosphorus pollutant hydrolyzed in the presence of the synthesized catalyst has been determined.

2. Experimental procedure

2.1. Materials

Zirconium tetrachloride compounds with 99.99% purity, 2-aminoterephthalic acid with 99% purity and dimethyl nitrophenyl phosphate with 99% purity were obtained from Sigma-Aldrich Company. Dimethylformamide (DMF) with a purity of 99%, chloroform with a purity of 99%, hydrochloric acid with a purity of 37%, acetic acid with a purity of 99%, N-ethylmorpholine with a purity of 99%, and 4-nitrophenoxide with a purity of over 99% were supplied by Merck Company. The absolute ethanol was purchased from Kimia Alkol Company as well.

2.2. Methods

The reactions were carried out in 25 and 100 ml vials. A Memmert VO-200 vacuum oven and a Yaxun YX3080 ultrasonic bath were used in catalyst synthesis. The materials were weighed on a Radwag AS22O scale with an accuracy of 0.1 mg. Using a Universal centrifuge model 37852, the reaction mixture was centrifuged. ARL Thermo-Xray device set at 20 kV and 20 mA was used for the Powder X-ray diffraction (PXRD) analysis. Fourier transform infrared spectra were obtained in cm^{-1} with a Thermo/Nicolet Magna-IR 550 device made by NICOLET Company with KBr tablets. The Brunauer-Emmett-Teller (BET) analysis was carried out using a NOVA E-series device. The absorbance was also measured using a GBC UV/VIS 911A device.

2.3. General synthesis procedure

A 25 ml vial was filled with 67 mg zirconium chloride salt and 5 ml dimethylformamide (DMF) solvent. For complete dissolution of the particles, the mixture was placed in an ultrasonic bath for 10 minutes after adding 0.5 ml of concentrated hydrochloric acid as a reaction catalyst. The vial was placed in the ultrasonic bath again for 20 minutes with 72 mg of 2-aminoterephthalic acid as ligand and 15 ml of DMF solvent. During this stage, all materials are dissolved in the solvent. After that, the caps of the containers were sealed, and the vials were placed in an oven at 100 °C. In about 2-3 hours, white catalyst particles appear inside the mixture. The vial was removed from the oven after 12 hours, and the excess solvent was separated. As a next step, the remaining solids were washed three times with DMF solvent before being centrifuged at 2500 rpm to separate the suspended solids from the solvent. The solids were washed three times with absolute ethanol (an alternative solvent with a lower boiling point than DMF solvent, 78.4 vs. 153 °C) to remove the trapped solvent and improve the porosity and capacity of the synthesized catalyst structure. Once again, centrifugation at 2500 rpm was used to separate the solids. Afterward, the catalyst was dried and weighed under a vacuum of 30 to 40 millibars at 100 degrees Celsius. Each synthesis test has been repeated three times to ensure reproducibility. Fig. 1 shows the reaction mixture at various stages of synthesis.

Fig. 1. From right to left: zirconium tetrachloride suspension before entering the ultrasonic bath, zirconium tetrachloride suspension after leaving the ultrasonic bath, catalyst formation about 2-3 hours after entering the oven, reaction mixture 12 hours after entering the oven (step out), final catalyst after washing with ethanol and drying

3. Results and Discussion

3.1. Optimization of catalyst synthesis

In this section, the optimization of the most important parameters affecting the catalyst synthesis, such as the reaction time, the reaction temperature, the amount of reaction solvent, type and the amount of acid catalyst required, type and quantity of the secondary solvent, and the rotation speed of centrifuges, has been discussed. These parameters were optimized using the monothetic analysis. This analysis, also known as one-factor-at-a-time (OFAT) or one-variable-at-a-time (OVAT) method, is a method of designing experiments involving the testing of factors, or causes, one at a time instead of multiple factors simultaneously. Also, the plots were prepared with the help of the MATLAB® software and other related software tools.

3.1.1. Optimization of the reaction time

At this stage, four separate experiments have been performed simultaneously and according to the general method mentioned in section 2.3 and the conditions listed in Table 2. Samples UI-001 to UI-003' were removed from the oven after 12, 24, 36, and 48 hours, respectively. The mass values of the catalysts obtained from each of these tests are shown in Table 2. The catalyst amount increased only 4% with a 100% increase in reaction time from 12 to 24 hours. The same increase in reaction time from 24 to 36 hours has resulted in a 29% increase in its amount. The amount of the catalyst decreased by 7.5% when the time increased from 36 to 48 hours.

Table 2. The amount of catalyst produced as a function of reaction time

Sample No.	Amount of zirconium chloride (mg)	Amount of ligand (mg)	Reaction temperature (°C)	Reaction time (hour)	Drying temperature (°C)	Amounts of the catalyst (mg)
UI-001	67	72	80	12	120	50
UI-002	67	72	80	24	120	52
UI-003	67	72	80	36	120	67
UI-003'	67	72	80	48	120	62

At different stages of optimization, the structure of synthesized catalysts was studied to evaluate the quality of their structure. The powder XRD patterns for samples UI-001, UI-002, and UI-003 are shown in Fig. 2. Despite the effect of the reaction time parameter on the amount of catalyst formed, this parameter does not affect the type or degree of crystallinity of the catalyst, and all three samples have the same pattern. A quantitative and qualitative comparison of the obtained catalysts indicates that a reaction time of 36 hours is the optimal reaction time for the 12 to 48 hours range.

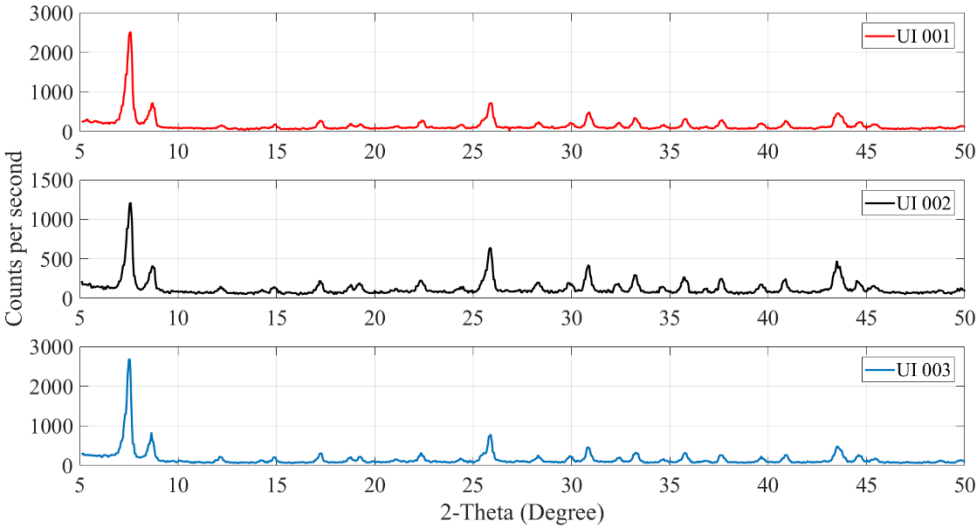

Fig. 2. Powder XRD pattern of samples UI-001, UI-002, UI-003 (synthesis conditions according to Table 2)

3.1.2. Optimization of the reaction temperature

In this stage, six experiments were planned and executed simultaneously according to the general method mentioned in section 2.3 and the conditions in Table 3. Three levels of reaction temperature were investigated at 80, 100, and 120 ºC, as well as two time levels of 12 and 36 hours (optimum time determined in section 3.1.1). Both reaction times of 12 hours and 36 hours produced higher amounts of the catalyst at 100 ºC. The maximum value of the UiO-66-NH_2 was obtained at 100 ºC and 36 hours of reaction time.

In a similar manner to section 3.1.1, the structures of the catalysts obtained from tests mentioned in Table 3 were compared. The powder XRD pattern of UI-003 and UI-010 samples (upper and lower temperature limits in the optimal value of the time parameter) as well as the zirconium tetrachloride composition pattern can be seen in Fig. 3. A bifurcated protrusion can be seen in the pattern of relative intensity on the irradiation angle of zirconium tetrachloride compound and in a part of the angle 10 to 15 degree. This is due to zirconium tetrachloride's structure. The XRD patterns of two samples UI-003 and UI-010 do not show this protrusion. As the reaction progresses, zirconium tetrachloride is no longer present as a raw material. Additionally, both patterns are similar to a large extent at temperatures of 80 and 120 degrees Celsius. These samples do not contain the zirconium-chlorine bond, indicating that the Zr-Cl bond has broken.

Table 3. The effect of the reaction temperature parameter on the amount of the resulting catalyst

Sample No.	Amount of zirconium chloride (mg)	Amount of ligand (mg)	Reaction temperature (°C)	Reaction time (hour)	Drying temperature (°C)	Amounts of the catalyst (mg)
UI-001	67	72	80	12	120	50
UI-004	67	72	100	12	120	85
UI-009	67	72	120	12	120	76
UI-003	67	72	80	36	120	67
UI-004'	67	72	100	36	120	89
UI-010	67	72	120	36	120	72

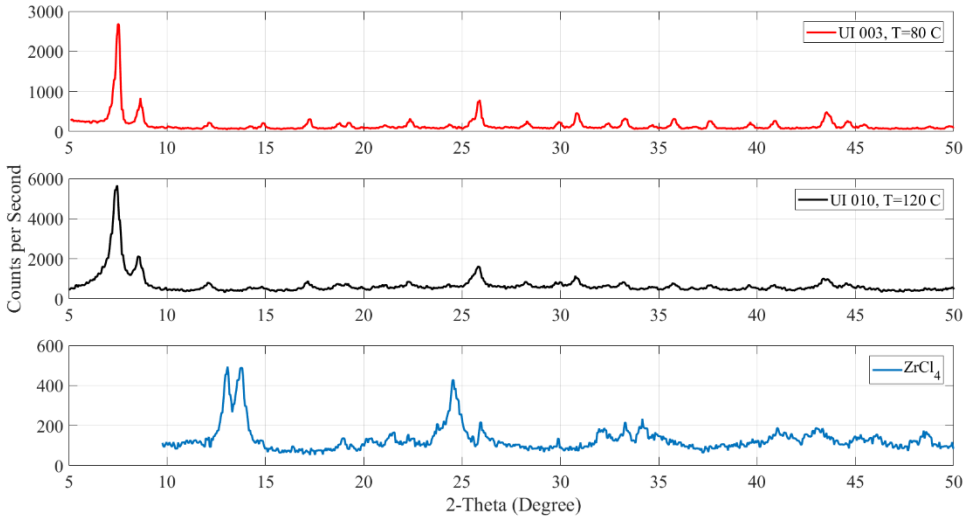

Fig. 3. Powder XRD pattern of UI-003 and UI-010 samples and zirconium tetrachloride composition (synthesis conditions according to Table 3)

Fig. 4 compares the infrared spectra (IR) of sample UI-004', $ZrCl_4$ compound and 2-aminoterephthalic acid ligand. This figure shows a peak of amine and acid groups in the range of 2500-3500 and a peak of the carbonyl group of the ligand compound. The fingerprint area of the product differs from the ligand and $ZrCl_4$ compounds used, indicating the presence of a new substance (target catalyst).

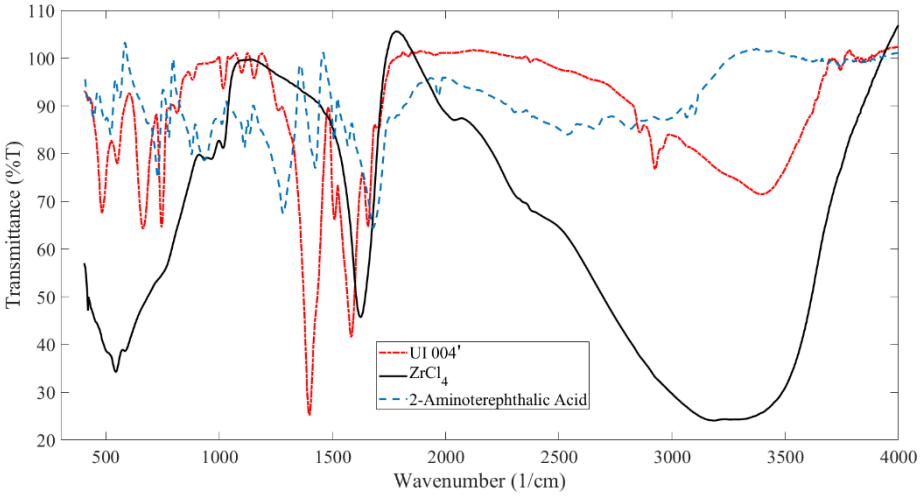

Fig. 4. IR spectrum of the synthesized catalyst (test UI-004') and the zirconium chloride and 2-aminoterephthalic acid ligand

According to Fig. 5, the UI-004' catalyst (see Table 3) displays similar IR spectra to those reported in references [30, 31]. The IR spectrum of the synthesized catalyst matches very well with the spectra reported in these references. A favorable match is observed between the reference spectrum and the synthesized catalyst based on the marked sharp peaks, which indicates the bond between the metal and the ligand. Fig. 6 also compares the XRD pattern of sample IU-003 with those reported in the references [30, 31]. XRD patterns also match very well in this comparison.

Table 4 compares the BET results of samples UI-003, UI-004', and UI-010. Due to the smaller average diameter of the pores formed in UI-004' catalyst than in other synthesized samples, this sample has the maximum specific area value of 824.75 m^2/g. The total pore volume in this sample is also higher.

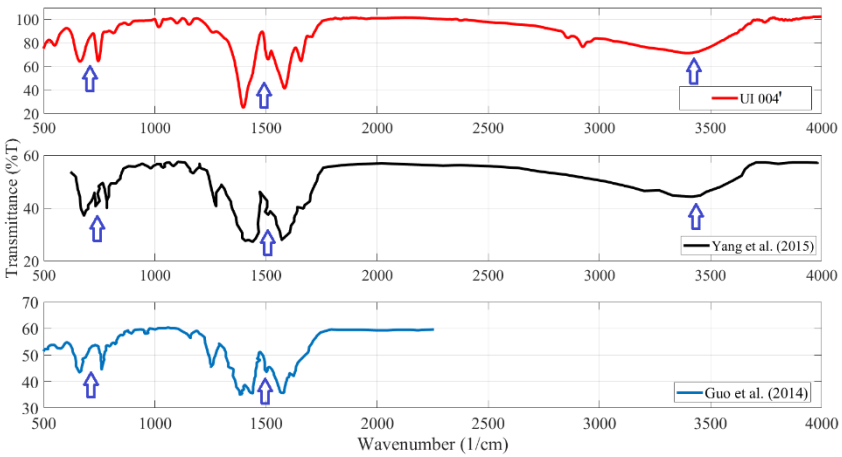

Fig. 5. A comparison of the IR spectrum of the synthesized metal-organic framework (sample UI-004') with that reported in references [30] and [31]

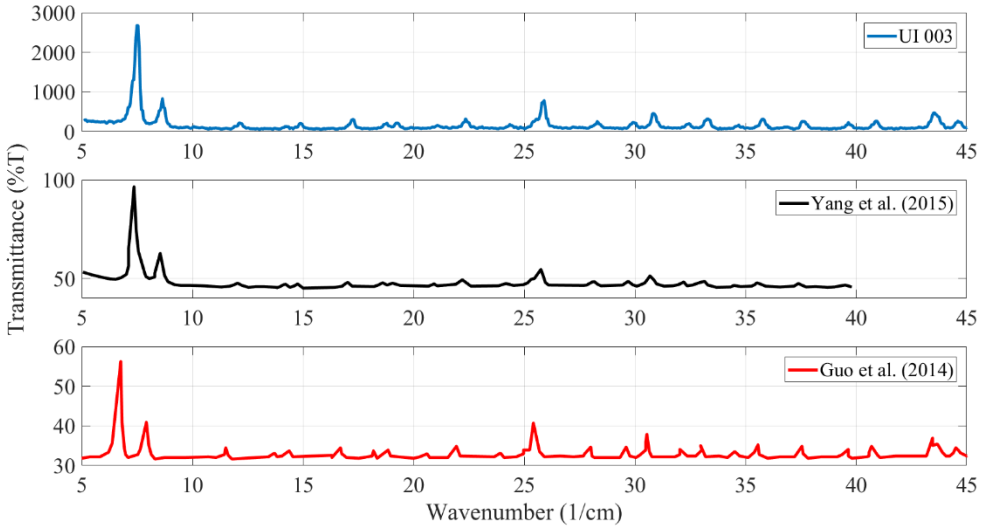

Fig. 6. The XRD pattern of the synthesized metal-organic framework (sample IU-003) and the pattern reported in references [30] and [31]

Table 4. Results of BET analysis on synthesized catalyst samples (synthesis conditions in Table 3)

Samples	Specific area (m^2 g^{-1})	Total pore volume (cm^3 g^{-1})	Mean pore diameter (nm)
UI-003	559.48	0.3461	2.4745
UI-004’	824.75	0.4631	2.2461
UI-010	600.44	0.3783	2.5200

3.1.3. Solvent amount optimization

According to Fig. 7, catalyst production efficiency is influenced by the amount of reaction solvent. The vertical axis represents efficiency relative to 100% catalyst production efficiency (corresponding to 20 ml of DMF solvent per 67 mg zirconium chloride). In amounts greater than 20 ml, the catalyst production efficiency does not change. Meanwhile, reducing the amount of solvent to less than 20 ml has decreased efficiency. Because of the inability of the raw materials to dissolve completely in small quantities of DMF solvent, the reaction has not been completed and its efficiency has been reduced. As can be seen, the optimal amount of solvent for optimum catalyst synthesis efficiency is 20 ml per 67 mg of zirconium chloride. This is the main reason for using 20 ml of DMF solvent mentioned in the general method of catalyst synthesis (see Section 2.3).

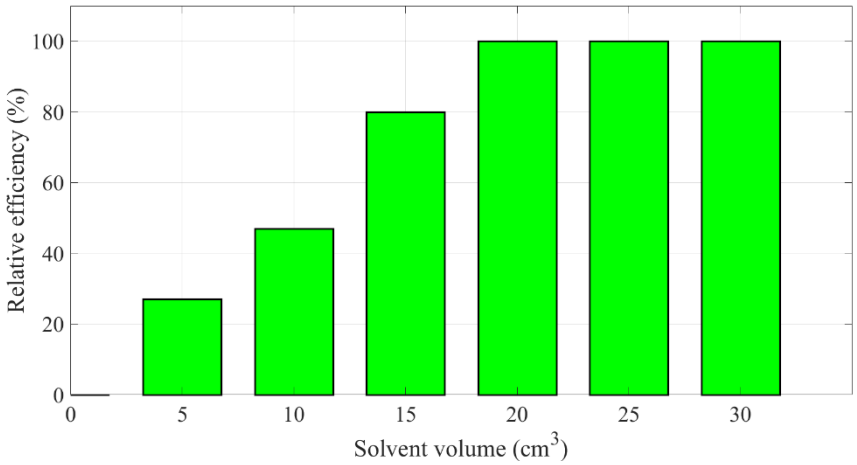

Fig. 7. The effect of the amount of reaction solvent on the relative efficiency of catalyst production (basis: 100% efficiency corresponding to 20 ml of DMF solvent per 67 mg zirconium chloride)

3.1.4. Acid catalyst optimization

By increasing the dissolution rate of the raw materials in the reaction mixture, acid catalysts accelerate the reaction and improve catalyst production efficiency. Therefore, the type and amount of acid catalyst needed were further investigated. Two experiments with the same synthesis conditions were initially conducted using two different acid catalysts (hydrochloric acid and acetic acid). The BET analysis of the resulting metal-organic frameworks indicates a much lower specific area of the MOF obtained from the acetic acid catalyst than the MOF obtained from hydrochloric acid (513.9 versus 824.8 m^2/g). Due to the inability of acetic acid to dissolve the raw materials completely, a gel suspension formed in the reaction mixture, which greatly reduced the speed and efficiency of MOF synthesis. Using the same synthesis conditions (similar to the synthesis conditions of sample UI-004' in Table 3) and three different amounts of concentrated hydrochloric acid (values of 0.25, 0.50, and 0.75 ml per 67 mg of zirconium chloride) were used to test the effects of the amount of acid catalyst.

Hydrochloric acid amounts of 0.50 and 0.75 ml did not significantly affect the efficiency or properties of MOF synthesized. Meanwhile, the decrease in the amount of hydrochloric acid from 0.50 to 0.25 ml, due to the decrease in the dissolution rate of raw materials in the reaction mixture, reduces the MOF production efficiency. In addition, the decrease in the amount of acid due to the lack of favorable reaction conditions leads to an unfavorable catalyst structure. According to the BET analysis of the catalyst resulting from 0.25 ml of hydrochloric acid, it has a specific area of 284.93 m^2/g and a mean pore diameter of 3.6598 nm, which is significantly less than the characteristics of the UI-004' sample (see Table 4).

3.1.5. Secondary solvent optimization

The secondary solvent serves two basic functions in the present synthesis. Due to washing the synthesized metal-organic framework, impurities are removed (or reduced) from its structure, resulting in purer crystals. By choosing a secondary solvent with a lower boiling point than the synthesis solvent (i.e., DMF), the second solvent in the catalyst washing step can also replace the DMF solvent trapped in the MOF structure and due to its greater volatility, it is more efficient to dry and activate the synthesized catalyst. More porosity and the specific area will be achieved by facilitating and improving the evaporation process.

To determine the most suitable secondary solvent, chloroform (with a boiling point of 61.2 °C) and absolute ethanol (with a boiling point of 78.4°C) were studied. The synthesis conditions in this section are similar to those mentioned for sample UI-004' in Table 3. According to the results, chloroform solvent produces a catalyst with a higher specific area than absolute ethanol (847.11 m^2/g vs 824.75 m^2/g) due to its greater volatility. No significant differences were observed in the production efficiency of MOF synthesized with the two investigated secondary solvents. Despite the relative improvement of 2.7% in the specific area of the catalyst resulting from chloroform, absolute ethanol as a secondary solvent is suggested due to factors such as chloroform's higher toxicity and damage to the equipment used. This is the main reason for using absolute ethanol as a secondary solvent in the mentioned general synthesis method (see Section 2.3).

3.1.6. Centrifuge rotation speed optimization

A rotational speed of 1000, 1500, 2000, 2500, 3000, and 3500 rpm was used to separate the synthesized MOF from the reaction mixture. Other synthesis conditions in this section are similar to those mentioned in Table 3 for sample UI-004'. Fig. 8 shows the results of this study. At rotation speeds of less than 2500 rpm, part of the solid catalyst remained in the reaction mixture as a suspension due to inefficient separation. Thus, 2500 rpm was selected as the optimal value for this parameter.

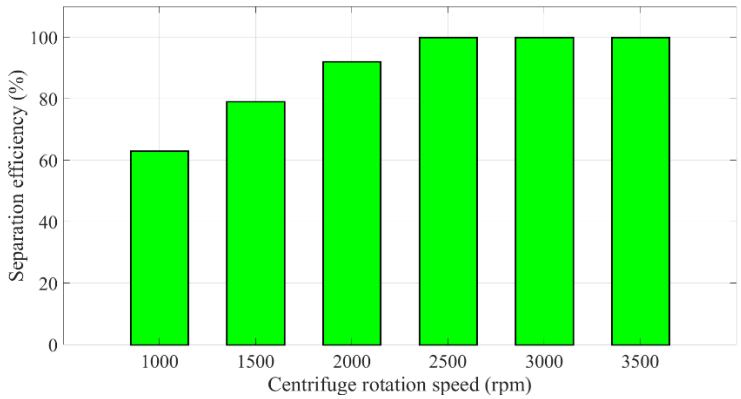

Fig. 8. The effect of centrifuge rotation speed on catalyst separation efficiency (synthesis conditions similar to UI-004' sample conditions in Table 3)

From a practical point of view, the present optimization in catalyst production, can accelerate commercialization and reduce catalyst production costs, which have been not explored in previous studies. For example, as it can be seen in Table 3, the catalyst production efficiency increased by 70% when the reaction temperature increased from 80 °C (one of the most commonly used temperature in the laboratory scale production [32]) to 100 °C, that means a production process with higher profit (compare the first and second rows in Table 3).

Also, in this study, by defining and scoring five industrial screening criteria, such as the price of required raw materials, the complexity of the synthesis reaction, the efficiency of the catalyst, the possibility of industrial production (scalability), as well as the cost of the necessary equipment (see Table 1), the best catalyst for the decomposition of the organophosphorus pesticides in commercial scales was determined. Furthermore, the studied catalyst has an excellent stability against water (moisture) and air that is often desired for practical productions, storages and usages, especially in water and wastewater treatments.

3.2. Experimental performance of the synthesized catalyst

After optimizing the synthesis of the target catalyst and its identification and characterization, the synthesized catalyst's performance in removing organophosphorus compounds was evaluated. An aqueous solution of dimethyl nitrophenyl phosphate (paraoxon-methyl, POM) was investigated for this purpose. Fig. 9 shows the decomposition of this organophosphorus compound in the presence of a synthesized catalyst. During hydrolyzing and destroying this compound, a secondary compound of 4-nitrophenoxide is formed, which is highly absorbent in the visible ultraviolet spectrum [33]. Therefore, the UV-VIS absorption can be easily used to measure the amount of formed 4-nitrophenoxide. In the present study, this is the most important reason for choosing POM organophosphorus compound.

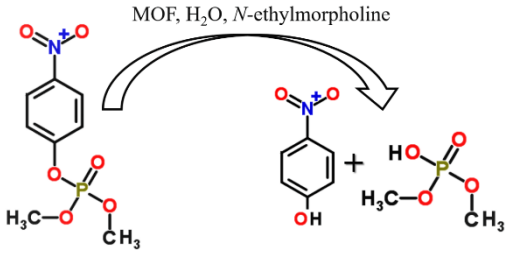

Fig. 9. The decomposition of POM compound in the presence of synthesized catalyst and the formation of 4-nitrophenoxide compound [33]

3.2.1. Organophosphorus pollutant removal test method

In a 1000 ml volumetric flask, 57 ml of N-Ethylmorpholine compound was added and diluted to 1000 ml with deionized water. 10 ml of the prepared solution was transferred to 25 ml vials after complete mixing. A magnet was used to stir 125 mg of the synthesized MOF with 5 ml of N-Ethylmorpholine solution for 30 minutes in a 10 ml vial. Then, 20 microliters of POM organophosphorus compound was added to this vial.

At certain time intervals, 20 microliters of the reaction mixture at room temperature were taken out of this vial and transferred into prepared 25 ml vials. At a wavelength of 408 nm, the absorbance of the solutions in these 25 ml vials was measured and recorded. In the UV-VIS blank (control) test tube, the solution contained in the 1000 ml balloon was used. The resulting absorption values are shown in Fig. 10. The concentration-absorption calibration curve of 4-nitrophenoxide in 0.45 M N-Ethylmorpholine solution was used to determine the half-life time ($t_{1/2}$) of pollutant decomposition. The flattening of the absorption graph in Fig. 10 following 60 minutes from the start of the reaction indicates the end of 4-nitrophenoxide formation, or the maximum removal of the investigated pollutant. Similar results have been reported by Zhao et al. [33]. Their findings show a 98% POM removal after 60 minutes of reaction time.

The amount of absorption measured in 60 minutes (2.1 a.u.) represents the decomposition and removal of 98% of the POM pollutant in the studied aqueous solution. Fig. 10 shows the time dependence of the measured percentage of POM removal based on the absorption values and the linear behavior observed in the concentration-absorption calibration curve of 4-nitrophenoxide compound. According to this diagram, the half-life time ($t_{1/2}$) of the decomposition of POM in the presence of the studied MOF is about 9 minutes. Mondloch et al. have reported half-life times of 1.5, 15, and 45 minutes, respectively, for the decomposition of this pollutant in the presence of dehydrated NU-1000, NU-1000, and UiO-66 metal-organic structures [34]. Although Moon et al. [35] and Katz et al. [36] have reported the reaction half-lives of 35 and 45-50 minutes, respectively, for decomposition of POM in the presence of UiO-66 structure.

Peterson et al. shown an excellent correlation between the p-NMR spectroscopy and UV−Vis method for estimation of the half-life time of the decomposition of POM in the presence of UiO-66 and UiO-66-NH_2 structures [37]. Further testing established that different rate-assessment techniques yield similar values for degradation half-lives. Also, their findings revealed that the best catalyst (UiO-66-NH_2) yields half-life of 0.7 minute (calculated based on UV−Vis method) and 0.9 minute (calculated based on p-NMR spectroscopy). A half-life time of 1 minute has been reported by Katz et al. [38] for decomposition of POM in the presence of UiO-66-NH_2 structure. However, Zhao et al. reported a half-life of 7.3 minutes for the POM pollutant degradation in the presence of UiO-66-NH_2 structure loaded on TiO_2-coated polyamide-6 nanofibers (PA-6@TiO_2@UiO-66-NH_2) [33] that is in good agreement with the present results.

Using the half-life time of 9 minutes of the hydrolysis reaction in the presence of this catalyst in comparison with the above reported values, it is shown that this structure accelerates the organophosphorus compound hydrolysis reaction.

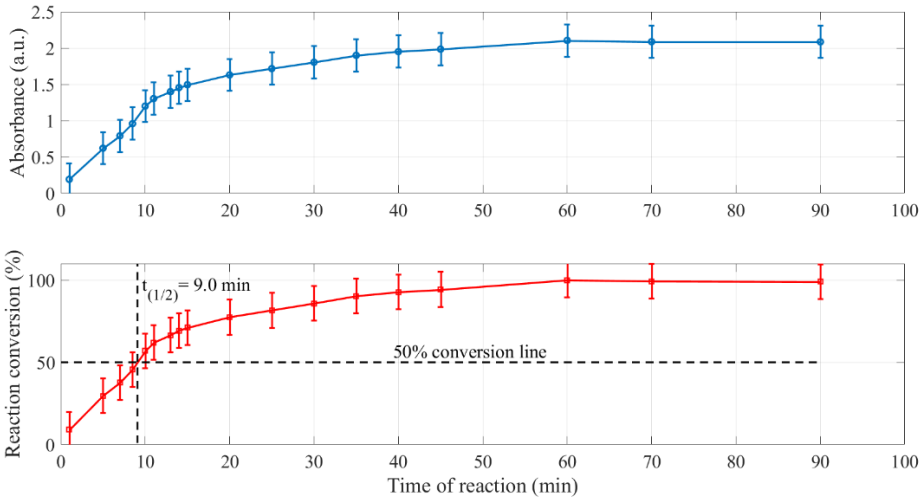

Fig. 10. Adsorption of 4-nitrophenoxide compound resulting from the hydrolysis reaction (top), time-dependent removal percentage of pollutant by synthesized catalyst (bottom)

4. Conclusion

In this work, unlike the previous studies, the optimum states of major variables affecting the solvothermal method in synthesizing the UiO-66-NH_2 structure, were determined. By considering the catalyst production yield as an objective function, the optimum values of the reaction time, reaction temperature, and amount of reaction solvent (i.e. DMF solvent) were obtained as 36 hr., 100 ^oC and about 0.296 ml solvent per mg of zirconium chloride (reactant). Furthermore, the optimum amount of acid catalyst required and rotation speed of centrifuges were found as about 7.5 µl per mg of zirconium chloride and 2500 rpm respectively. Also, the present findings revealed that, in an aqueous environment, the synthesized catalyst can be able to decompose about 98% of dimethyl nitrophenyl phosphate (as a representative of organophosphorus pesticides) in less than one hour. Finally, the half-life time of the decomposition of this pollutant in the presence of the catalyst was found as about 9 minutes, which appeared to be in good agreement with earlier published data for UiO-66-NH_2 structure loaded on TiO_2-coated polyamide-6 nanofibers (a half-life of 7.3 minutes).

References

1. Khodadadi M, Samadi MT, Rahmani AR, (2011). Comparison between the efficiency of advanced oxidation process and coagulation for removal organophosphorus and carbamat pesticides (in Farsi). Iran. J. Health & Environ., pp: 4:277-287.
2. Gissawong N, Mukdasai S, Boonchiangma S, Sansuk S, Srijaranai S, (2020). A rapid and simple method for the removal of dyes and organophosphorus pesticides from water and soil samples using deep eutectic solvent embedded sponge. Chemosphere, pp: 260:1-9.
3. Maria CV, Andreas SP, (2020). Recent advances on the removal of priority organochlorine and organophosphorus biorecalcitrant pesticides defined by Directive 2013/39/EU from environmental matrices by using advanced oxidation processes: An overview (2007–2018). Journal of Environmental Chemical Engineering, pp: 8:xxx-xxx.
4. Sefidkar R, Mazloomi SM, (2014). A Review of the effects of different types of food processing methods on the amount of pesticides residues in raw and processed plant-based food (in Farsi). Journal of Ilam University of Medical Sciences, pp: 22: 24-32.
5. Gholipoor M, Shokrzadeh M, Esfahenezadeh MH, Karemzadeh L, Ebrahemmagam B, Salehifar E, Enayati AA, (2014). Assessment of organophosphorus residues together in strawberry produced in mazandaran, Iran (in Frasi). J Mazand Univ Med Sci., pp: 24:92-102.
6. Mahmoudi GA, Asaee R, (2008). Epidemiologic study of Organophosphate and Organochlorate pesticides poisoning in hospitalized patients in khorramabad Shohada Ashayer hospital from Mars to August 2006 (in Farsi). Yafte, pp: 10:3-10.
7. Talebi Kh, Ebadollahi AR, Mirhadi SA, Madani, R, Emami Yeganeh B, (2001). Determination of coumaphos residues in honey from some apiaries in Tehran province (in Farsi). Applied Entomology and Phytopathology, pp: 68: 73-83.
8. Yazdi Z, Sarreshtehdari M, Zohal MA, (2011). Respiratory disorders in workers in contact with organophosphorus substances (in Farsi). Medical Journal of Mashhad, pp: 53:206-213.
9. Rafati M, Moghaddam Nia AA, (2010). Organophosphorus Compounds Poisoning (in Farsi). J Babol Univ Med Sci, pp: 12:71-85.
10. Bakouri HE, Morillo J, Usero J, Ouassini A, (2008). Potential use of organic waste substances as an ecological technique to reduce pesticide ground water contamination. Journal of Hydrology, pp: 353: 335–342.
11. Samadi MT, Khodadadi M, Rahmani AR, Allahresani A, Saghi MH, (2011). Comparison of the efficiency of simultaneous application of UV/O3 for the removal of organophosphorus and carbamat pesticides in aqueous solutions (in Farsi). Journal of Water and Wastewater, pp: 1:69-75.
12. Yu JJ, (2002). Removal of organophosphate pesticides from wastewater by supercritical carbon dioxide extraction, Water Research. Pp: 36:1095–1101.
13. Dehghani MH, Shariati Niasar Z, Mehrnia MR, Shayeghi M, Al-Ghouti MA, Heibati B, McKay G, Yetilmezsoy Kh, (2017). Optimizing the removal of organophosphorus pesticide malathion from water using multi-walled carbon nanotubes. Chemical Engineering Journal, pp: 310:22–32.
14. Guivarch E, Oturan N, Oturan MA, (2003), Removal of organophosphorus pesticides from water by electrogenerated Fenton's reagent. Environ Chem Lett, pp: 1:165–168.
15. Kamboh MA, Ibrahima WAW, Nodeha HR, Sanagia MM, Sherazid STH, (2016). Removal of selected organophosphorus pesticides from water using newly fabricated amino-substituted calixarene-based magnetic sporopollenin. New J. Chem., pp: 40:3130-3138.

16. Costa RO, Barcellos PS, Canela MC, (2018). Removal of pesticide residues after simulated water treatment: by-products and acetylcholinesterase inhibition. Eclética Química, PP: 43:65-73.
17. Dyguda-Kazimierowicz E, Roszak S, Sokalski WA, (2014). Alkaline hydrolysis of organophosphorus pesticides: the dependence of the reaction mechanism on the incoming group conformation. J. Phys. Chem. B, pp: 118:7277−7289.
18. Aly OA, Badawy MI, (1982). Hydrolysis of organophosphate insecticides in aqueous media. environment international, pp: 7:373-377.
19. Lee YR, Kim J, Ahn WS, (2013). Synthesis of metal-organic frameworks: A mini review. Korean J. Chem. Eng., pp: 30:1667-1680.
20. Hupp JT, Farha OK, Katz MJ, Mondloch JE, (2016). Metal organic frameworks for the catalytic detoxification of chemical warfare nerve agents. US Patent, patent number: 2016/0175827 Al.
21. Liu Y, Howarth AJ, Vermeulen NA, Moon SY, Hupp JT, Farha OK, (2017). Catalytic degradation of chemical warfare agents and their simulants by metal-organic frameworks. Coordination Chemistry Reviews, pp: 1:101-111.
22. Griffin SL, Champness NR, (2020). A periodic table of metal-organic frameworks. Coordination Chemistry Reviews, pp: 414:1-20.
23. Bai Y, Dou Y, Xie LH, Rutledge W, Li JR, Zhou HC, (2016). Zr-based metal–organic frameworks: design, synthesis, structure, and applications. Chem. Soc. Rev., pp: 45:2327-2367.
24. Zhang H, Xiong P, Li G, Liao Ch, Jiang G, (2020). Applications of multifunctional zirconium-based metal-organic frameworks in analytical chemistry: Overview and perspectives. Trends in Analytical Chemistry, pp: 131:1-16.
25. Ahmad Kh, Nazir MA, Qureshi AK, Hussain E, Najam T, Javed MS, Shah SSA, Tufail MK, Hussain Sh, Khan MA, Shah HR, Ashfaq A, (2020). Engineering of Zirconium based metal-organic frameworks (Zr-MOFs) as efficient adsorbents. Materials Science & Engineering B, pp: 262:1-11.
26. McKinstry C, Cussen EJ, Fletcher AJ, Patwardhan SV, Sefcik J, (2017). Scalable continuous production of high quality HKUST-1 via conventional and microwave heating. Chemical Engineering Journal, pp: 326:570–577.
27. Dunne PW, Lester E, Walton RI, (2016). Towards scalable and controlled synthesis of metal–organic framework materials using continuous flow reactors. React. Chem. Eng., pp: 1:352-360.
28. Martinez MR, Batten MP, Polyzos A, Carey KC, Mardel JI, Lim KS, Hill MR, (2014). Versatile, high quality and scalable continuous flow production of metal-organic frameworks. Scientific Reports, pp: 4:5443.
29. Adschiri T, Kanazawa K, Arai K, (1992). Rapid and continuous hydrothermal crystallization of metal oxide particles in supercritical water. J. Am. Ceram. Sor., pp: 75:1019-1022.
30. Yang J, Dai Y, Zhu X, Wang Z, Li Y, Zhuang Q, Shi J, Gu J, (2015). Metal–organic frameworks with inherent recognition sites for selective phosphate sensing through their coordination-induced fluorescence enhancement effect. J. Mater. Chem. A, pp: 3:7445.
31. Guo Zh, Xiao Ch, Maligal-Ganesh RV, Zhou L, Goh TW, Li X, Tesfagaber D, Thiel A, Huang W, (2014). Pt nanoclusters confined within metal−organic framework cavities for chemoselective cinnamaldehyde hydrogenation. ACS Catal., pp: 4:1340−1348.

32. Wang T, Han L, Li X, Chen T, Wang S, (2022). Functionalized UiO-66-NH2 by trimellitic acid for highly selective adsorption of basic blue 3 from aqueous solutions. Frontier in Chemistry, pp: 962383:1-13
33. Zhao J, Lee DT, Yaga RW, Hall MG, Barton HF, Woodward IR, Oldham CJ, Walls HA, Peterson GW, Parsons GN, (2016). Ultra-fast degradation of chemical warfare agents using MOF–nanofiber kebabs. Angew. Chem., pp: 128:1–6.
34. Mondloch JE, Katz MJ, Isley III WC, Ghosh P, Liao P, Bury W, Wagner GW, Hall MG, DeCoste JB, Peterson GW, Snurr RQ, Cramer ChJ, Hupp JT, Farha OK, (2015). Destruction of chemical warfare agents using metal–organic frameworks. Nat Mater, pp: 14:512-516.
35. Moon SY, Liu Y, Hupp JT, Farha OK, (2015). Instantaneous Hydrolysis of Nerve-Agent Simulants with a Six-Connected Zirconium-Based Metal–Organic Framework. Angew. Chem., pp: 127:6899-6903.
36. Katz MJ, Mondloch JE, Totten RK, Park JK, Nguyen ST, Farha OK, Hupp JT, (2014). Simple and Compelling Biomimetic Metal–Organic Framework Catalyst for the Degradation of Nerve Agent Simulants. Angew. Chem. Int. Ed., pp: 53:497-501.
37. Peterson GW, Moon SY, Wagner GW, Hall MG, DeCoste JB, Hupp JT, Farha OK, (2015). Tailoring the Pore Size and Functionality of UiO-Type Metal−Organic Frameworks for Optimal Nerve Agent Destruction. Inorg. Chem., pp: 54, 9684-9686.
38. Katz MJ, Moon SY, Mondloch JE, Beyzavi MH, Stephenson CJ, Hupp JT, Farha OK, (2015). Exploiting parameter space in MOFs: a 20-fold enhancement of phosphate-ester hydrolysis with UiO-66-NH2. Chem. Sci., pp: 6, 2286-2291.